Abstract Concentrated, approximately close-packed populations of the swimming bacteria *Bacillus subtilis* form a collective dynamic phase. This "Zooming BioNematic" (ZBN), exhibits long-range order, analogous to the molecular alignment of nematic liquid crystals, coupled with remarkable spatial and temporal correlations of velocity and vorticity, as measured with PIV. The appearance of quasi-turbulence in a nominally Stokes Flow system can be understood by accounting for the local energy input by the swimmers, with a new dimensionless ratio, analogous to the Reynolds number. The interaction between organisms and boundaries, and with one another, is modeled by application of the methods of regularized Stokeslets.

Noname manuscript No.
(will be inserted by the editor)

Luis H. Cisneros[1], Ricardo Cortez[2], Christopher Dombrowski[1], Raymond E. Goldstein[1,3] and John O. Kessler[1]

Fluid dynamics of self-propelled micro-organisms, from individuals to concentrated populations.

the date of receipt and acceptance should be inserted later

1 Introduction

The fluid dynamics of "fast, large" self-propelled objects, ranging from krill to whales, mosquitoes to eagles, is extensively studied and intuitively understood. In these cases the Reynolds number Re ranges from somewhat >1 to enormous. Monocellular bacteria, algae, protists, are microscopic. Although some of them swim many body lengths per second, $Re \ll 1$. The flows associated with locomotion hydrodynamically couple the swimmers to each other and to nearby surfaces. They can also generate significant advective transport of molecular solutes associated with life-processes (Solari *et al.*, 2006; Short *et al.*, 2006).

Much micro-bio-hydrodynamical research has focused on the morphologically similar swimming bacteria *Escherichia coli, Salmonella typhymuris* and *Bacillus subtilis*. The chief experimental results and theoretical insights described in this paper are derived from our investigations of individual and collective swimming phenomena of *B. subtilis*.

Individual cells of these generally non-pathogenic soil bacteria are rod-shaped (see Fig. 1). Their length ranges from two to eight micrometers, depending on nutrition and growth stage. In typical experiments they are approximately 4 μm long and somewhat less than 1 μm in diameter. They are peritrichously flagellated: the helical flagella, their means of propulsion, are distributed randomly over the cell body. These structures emerge from motors that are fixed within the cell membrane. The shafts are able to rotate at various rates, typically in the order of 100 Hz. The flagella are complex polymeric structures approximately 20 nm in diameter. Their length is 10-15 μm, considerably longer than a cell's body. The flagella are attached to the motors by a flexible hook which acts as a universal joint. The pitch of the helices is ~ 4 μm. Fig. 1 shows two cells caught in the process of dividing. When a bacterial cell swims smoothly forward, hydrodynamic interactions between the many helical flagella cause the formation of a propulsive bundle within which they co-rotate. The swimming speed of an individual is approximately 11% of the helix wave speed (Magariyama *et al.*, 1995 and 2001). The motors are fueled by proton gradients. The rotation direction of the motors is reversible. The reversal frequency is a function of the surrounding concentration of chemicals and of other factors. It can play a major role in chemotaxis (Berg, 1993; Berg, 2003). The cell bodies are not polar. The flagellar bundle can form at either end of a cell, an important aspect of group locomotion, discussed in section 5.

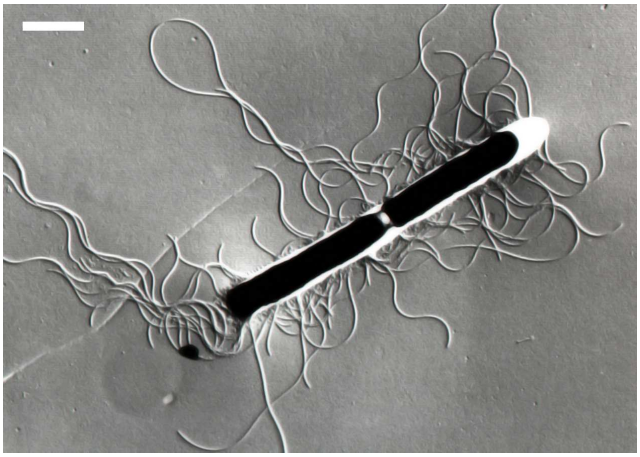

Fig. 1 Two *Bacillus subtilis* cells about to divide. White bar on the left side is 1 μm long. Flagella can be seen emerging from the body. Many of them have been broken during sample preparation for this transmission electronmicrograph.

Because $Re \ll 1$, a single swimming bacterium has associated with it an extensive flow field which is pro-

1- Department of Physics, University of Arizona, 1118 E. 4th St., Tucson, AZ 85721;
2- Department of Mathematics, Tulane University, 6823 St. Charles Ave., New Orleans, LA 70118;
3- Department of Applied Mathematics and Theoretical Physics, Centre for Mathematical Sciences, University of Cambridge, Wilberforce Road, Cambridge CB3 0WA, UK

duced entirely by the drag forces on the fluid, exerted forward by the cell body and backward by the flagella. No wake remains behind moving cells or cell groups. When a cell stops rotating its flagella, all motion of the fluid and of the cell ceases. Motor boats are not analogs. The viscous forces are described by Slender Body Theory and extensions of Faxén's and Stokes' laws (Pozrikidis, 1997). For an isolated swimmer, the net propulsive force of the flagella must equal the opposing drag force of the body connected to the flagella, taking into account the effect of nearby surfaces, or other organisms. The solutions of the relevant creeping flow equations are linear and time reversible. Under actual, real world situations, these conditions are only approximate or worse. Deviations from the ideal occur when flows affect boundary conditions such as location and orientation of nearby cells, the speed and directionality of flagella beating, the deformation of nearby interfaces.

The fluid dynamics of suspensions of living organisms can be modified by their behavior. For example, we describe in section 4, that *B. subtilis* tend to swim upstream in a shear flow. Should we ascribe this to hydrodynamic interactions that passively orient cells which simply maintain rotating their flagella? Or perhaps might we infer that, when bacteria experience shear stress, they "want" to swim upstream? In section 4 we show one example of this phenomenon, adequate for the purpose of demonstrating its importance for recruiting individuals into groups of co-directionally swimming cells. However, the specific recorded trajectories of more than sixty cells show major differences in topological detail. The recruiting of cells into correlated groups does not depend on the origin of the ultimate behavior, but inferences concerning fundamentals of micro-bio-hydrodynamics require experiments designed to disentangle the physics from the biology. We are currently pursuing this objective.

Micro-organisms use, exude, and respond to the presence of biologically significant molecules. Chemical interactions provide an avenue for change of the collective dynamic. The consumption of dissolved molecules such as oxygen induces remarkable behavior of individual bacteria. For instance, swimming up oxygen concentration gradients, produced by a combination of consumption and diffusion supplied through a water/air interface, leads via hydrodynamics and gravitational (Rayleigh-Taylor) instability to the highly concentrated populations (Dombrowski *et al.*, 2004, Tuval *et al.*, 2005) which are the chief subject of this paper. Emission of molecules involved in signalling and exudates of biopolymers that may radically change the viscosity of the embedding fluid are both involved in quorum sensing (Miller *et al.*, 2001) and the formation of biofilms (Kolter *et al.*, 2006). Before occurrence of these radical events, subtle chemical interactions can influence the biology and modify the behavior of individual cells. Even at low concentrations, polymer exudates modify the properties of the suspension. For instance, we observe that in slightly aged cultures of still normally motile bacteria, passive marker particles, as well as the bacteria themselves, can be coupled by polymer strands of cellular origin. Furthermore, the water/air interface can accumulate bacterially-synthesized polymer surfactants that trap and immobilize bacteria arriving there. This nominally free surface becomes a stiff, no-slip boundary. In biofluid mechanics, before reaching definitive conclusions: *caveat emptor*.

An astonishing phenomenon, the Zooming BioNematic collective phase, occurs when the bacterial cells are very concentrated, i.e. nearly close-packed. They form codirectionally swimming domains that move chaotically, giving the appearance of turbulence. These regions may move at speeds much larger than the average speed of single organisms.

Maintenance of a sustaining environment is required when working with suspensions of living organisms. *B. subtilis* require oxygen for swimming. The dynamics of the ZBN phase, driven by swimming, continue unabated for hours, suggesting that an adequate supply of oxygen is available to the bacteria. Molecular transport into the bacterial suspension from the adjacent air involves molecular diffusion and also advection by collectively generated streaming. Bacteria consume $\sim 10^6$ molecules of O_2 per second per cell. As the solubility of oxygen is $\sim 10^{17}$ molecules/cm^3, and the concentration of cells is $\sim 10^{11}$cm^{-3}, in absence of transport into the suspension, the oxygen would be gone in about one second. During experiments on the ZBN, the typical depth of the suspension is $L \sim 5 \times 10^{-3}$cm. With the diffusion coefficient of O_2 in water $D = 2 \times 10^{-5}$cm^2/sec, the diffusion time, $L^2 D^{-1}$ is also of order one second. A scale for collective velocity is $V \sim 5 \cdot 10^{-3}$cm/sec, so that the advection time is again approximately one second. This fortuitous combination of characteristic times implies "just in time" oxygen delivery. The Peclet number, $P_e = LV/D$, is therefore of order unity. The complex and quite fascinating details of the transport processes of food, waste products, and of molecular signals need extensive investigation, another example of the convolution of biology and fluid dynamics. The biochemistry of metabolism and sensory processes also plays a major role. Recent works (Solari *et al.*, 2006; Short *et al.*, 2006) describe investigations on diffusive transport necessarily augmented by advection due to the motion of flagella. There, the context is an aspect of the origin of multicellularity in a family of algae. In a sense, the coherent, collective behavior of a bacterial population converts it too into a type of multicellular "individual."

2 Collective Phenomena: The Zooming BioNematic (ZBN)

The volume of one cell of *B. subtilis* is $\sim 1.5 \times 10^{-12}$cm^3. Since the bodies are rod-shaped, concentrated populations, e.g. $n \sim 10^{11}$cm^{-3}, tend to form domains within

which the self-stacked cell bodies are approximately parallel. The entire high concentration region consists of such domains. All the cells in one domain swim in the same direction, so that, unlike the analogous liquid crystals, the domains move and are dynamically polar. The cell bodies have no intrinsic polarity; on any one cell, the propelling flagella can flip to either end of the body/rod. This appears to be one mechanism for quorum polarity: individual organisms joining the swimming direction of the majority. A domain is thus characterized by coherence of body alignment, and polarity, i.e. coherence of swimming direction. The domains swim in arbitrary directions, they zoom about at speeds that often exceed the swimming speed of individual bacteria. These zooming domains spontaneously form and disintegrate, giving the appearance of internally maintained turbulence. The next section describes PIV measurements of spatial and temporal correlations of velocity, vorticity and polar alignment.

This phase of active microorganism motion is embedded in water. The entire dynamical system is driven by the rotation of the helical flagella that emerge from the bodies of the bacteria. The flagella propel (force) the fluid phase backward; they exert an equal and opposite force on the bodies from which they emerge. Since the flagella are typically three times longer than the cell bodies, the flow generated by the flagella of a particular cell exerts a backward drag on the bodies of several cells located behind that particular one. It therefore seems likely that the flows in the interior of domains are rather small, and that propulsion arises mostly at the periphery. Further discussion and relevant calculations follow in section 5, which also presents results on cohesive hydrodynamic interactions.

3 Coherence of polar and angular order: a novel use of PIV

Our experiments were conducted with *B. subtilis* strain 1085B suspended in terrific broth (TB) (Ezmix Terrific Broth, Sigma; 47.6 g of broth mix and 8 ml of glycerin in 1 liter of distilled water). Samples were prepared by adding 1 ml of $-20°$C stock to 50 ml of TB and incubating for 18 hours in a shaker bath at 37°C and 100 rpm. Then, 1 ml of bacteria suspension was mixed with 50 ml of fresh TB and incubated for another 5 hours.

A single drop of suspension was put on plastic petri dish to be observed under an inverted microscope with 20x bright field objectives. This magnification is enough to observe individual cells and produce a field of view reasonably wide. Additional water reservoirs were placed in the closed chamber to induce high humidity and avoid evaporative flows at the edge of the drop. The sessile drop is imaged from below through the bottom of the petri dish and close to the contact line, where dimensions of the medium are close to a thin layer and self-concentration mechanisms provide very high accumulations of cells (Dombrowski *et al.*, 2004). Videos where obtained using a high-speed digital camera (Phantom V5) at a rate of 100 frames per second and with a resolution of 512×512 pixels. Sets of 1000 frames were subsequently obtained from each of those videos and processed with a commercial particle-imaging-velocimetry system (DANTEC Flow Manager) in the cinemagraphic mode. The PIV system can estimate the most probable displacement of small rectangular regions in the image by implementing a simple pattern matching algorithm between two consecutive images (Willert *et al.*, 1991; Keane *et al.*, 1992). A sampling grid of 42×42 cells, each eight pixel wide with 25% overlap, was chosen. Given the displacement of these small evaluation regions at a given frame rate, a discrete and instantaneous velocity field is returned for each time step. Although the observed system is a thin layer, such measurements are projections of a three-dimensional field into the plane defined by the area of view and the optical depth of field.

Measurement of the coherence lengths and times that characterize the dynamics of the ZBN can be done by the implementation of a PIV analysis on the recorded motion of passive tracer particles, or of the suspended bacteria themselves. The data presented here uses the latter technique. Passive tracer data is too sparse when the concentration of tracer particles is sufficiently low so as not to affect the basic phenomena.

On the other hand, optical problems arise in the highly concentrated ZBN phase. The close-packed cells scatter light, producing distortion and diffraction effects that reduce the quality of the image. Individual cells are difficult to resolve in this setup. Though more work is needed to increase precision on velocity measures, analysing diffuse images with PIV is not necessarily a problem. This technique definitely captures well the overall dynamics of the system in a quantitative way.

An example snapshot of the velocity field is shown in Fig. 2. The corresponding vorticity field is shown in Fig. 3.

The motion of the suspension appears turbulent. Coherent regions, surges, plumes and jets occur intermittently. These domains of aligned motility are many hundreds of times larger than bacterial dimensions, remaining coherent for a second or longer. Observed cinematographically, the leading segments of such plumes often roll up into spirals, then disperse, either spontaneously or due to interactions with neighboring coherent regions. These observations relate to the trajectories, the paths of groups consisting of hundreds or thousands of bacteria. PIV provides only a quasi-instantaneous snapshot of streamlines associated with a velocity field derived from the data.

Correlation functions were estimated from the quantitative data. The temporal correlation function of velocity is defined as the following statistic over the vector

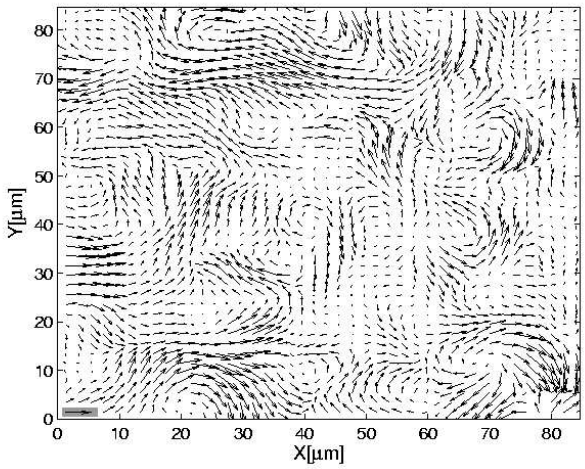

Fig. 2 One randomly chosen instant of the bacterial swimming vector field estimated by PIV analysis. The vector in the small gray rectangle in the lower left corner represents a magnitude of 50 μm/sec. The turbulent appearance of the flow is evident here.

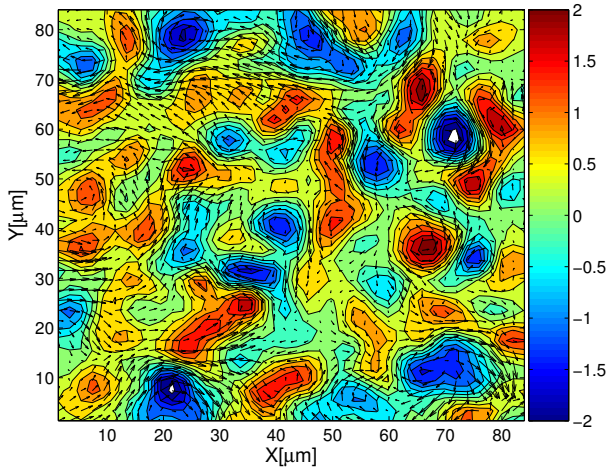

Fig. 3 Vorticity of the bacterial swimming velocity vector field. Color bar indicates vorticity values in $\sec^{-1}$. Fig. 4 (c) and (d) show correlations between adjacent regions of opposite handedness.

field $\mathbf{v}(\mathbf{x},t)$:

$$J_v(\mathbf{x},t) = \frac{\langle \mathbf{v}(\mathbf{x},s+t)\cdot\mathbf{v}(\mathbf{x},s)\rangle_s - \langle \mathbf{v}(\mathbf{x},s)\rangle_s^2}{\langle \mathbf{v}^2(\mathbf{x},s)\rangle_s - \langle \mathbf{v}(\mathbf{x},s)\rangle_s^2}. \quad (1)$$

The space correlation function is defined as

$$I_v(r,t) = \frac{\langle \mathbf{v}(\mathbf{x}+\mathbf{r},t)\cdot\mathbf{v}(\mathbf{x},t)\rangle_{\mathbf{x},\theta} - \langle \mathbf{v}(\mathbf{x},t)\rangle_{\mathbf{x}}^2}{\langle \mathbf{v}^2(\mathbf{x},t)\rangle_{\mathbf{x}} - \langle \mathbf{v}(\mathbf{x},t)\rangle_{\mathbf{x}}^2}, \quad (2)$$

where $\langle\cdot\rangle_s$ is the average over time frames and $\langle\cdot\rangle_{\mathbf{x}}$ indicates the average over space coordinates $\mathbf{x}=(x,y)$. The first term in Eq.(2) is also averaged over all possible angles θ of r. Then $I_v(r)$ depends only on the magnitude $r\equiv|\mathbf{r}|$.

Similar definitions are used for the correlation of the vorticity scalar field $\Omega(\mathbf{x},t)$,

$$J_\Omega(\mathbf{x},t) = \frac{\langle \Omega(\mathbf{x},s+t)\Omega(\mathbf{x},s)\rangle_s - \langle \Omega(\mathbf{x},s)\rangle_s^2}{\langle \Omega^2(\mathbf{x},s)\rangle_s - \langle \Omega(\mathbf{x},s)\rangle_s^2} \quad (3)$$

and

$$I_\Omega(r,t) = \frac{\langle \Omega(\mathbf{x}+\mathbf{r},t)\Omega(\mathbf{x},t)\rangle_{\mathbf{x},\theta} - \langle \Omega(\mathbf{x},t)\rangle_{\mathbf{x}}^2}{\langle \Omega^2(\mathbf{x},t)\rangle_{\mathbf{x}} - \langle \Omega(\mathbf{x},t)\rangle_{\mathbf{x}}^2}. \quad (4)$$

Using these measures on the PIV data, we obtain 1000 different curves for I_v and I_Ω, one for each time realization, and $42\times42 = 1764$ curves for J_v and J_Ω, one for each possible discrete coordinate in the PIV sampling grid. We further calculate averages of these sets to show the overall mean behavior of the correlation functions. Graphs are shown in Fig. 4. Comparison of the average plots with plots of individual cases show that, because of the prevalence of positive and negative correlations, averaging does not provide good insights for dynamic events. These oscillations of correlation are somewhat reminiscent of events at high Re.

These analyses reveal correlation lengths of velocity on the order of 10 μm, which is about a typical vortex radius in Fig. 3. We also observe *anti*correlation extending for more than 70 μm and coherence in time that persists for at least a second, suggestively close to the advection time mentioned at the end of section 1. While these measures define some characteristic length and time of the system, these curves do not provide information on the continuity and dominance of extensive coherence of alignment and collective polar motion. A novel method of analysis of the velocity field, using the streamlines derived from PIV was employed to provide that insight.

The local velocity of domains of concentrated bacteria correlates with the direction of the axis of the cell bodies. In this way, the direction of the associated streamlines averaged over suitably chosen areas can provide a measure of the orientation of a local director vector, traditionally used to characterize liquid crystalline phases. In this context, the swimming co-direction defines the polarity of coherent behavior absent from standard liquid crystalline order (de Gennes and Prost, 1993). Spatially rapid deviations of streamline directions from the local average provide a quantitative measure of the end of planar coherence. They may signal the occurrence of orientational singularities, such as excursions into the orthogonal dimension or the presence of boundaries that define unrelated regions of coherence that collide or fold into each other. Relatively low angle deviations of the director provide data on the splay and bend parameters that occur in the analysis of the liquid crystal energy function.

We now introduce a new method of analysis which consists of defining a suitable scalar field to measure the

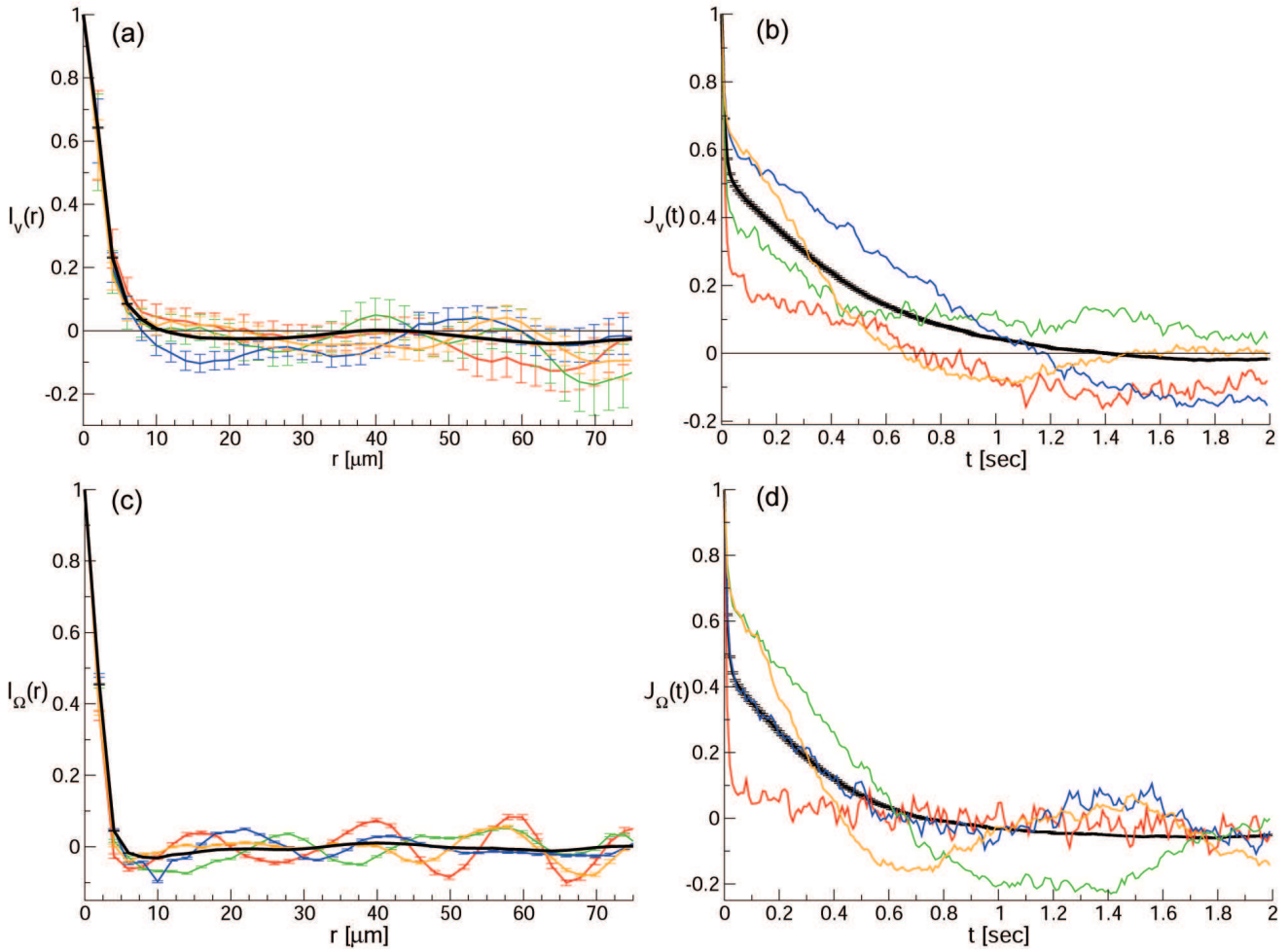

Fig. 4 (a) Velocity space correlation function $I_v(r)$. Four examples corresponding to four different times are shown in colors; the black trace is the average over 1000 time realizations. (b) Velocity time correlation function $J_v(t)$. Four examples corresponding to four particular locations in the field of view are shown in colors. Black is the average over space. Plots are show for the vorticity space correlation $I_\Omega(r)$ (c) and time correlation $J_\Omega(t)$ (d) are shown for four examples and, again in black, for the average: The oscillations in (c) correspond to alternation of handedness of vorticity, shown in Fig. 3.

level of coherent directional motion in the velocity field. The obvious choice is a local average $\Phi_R = \langle \cos\theta \rangle_R$ of the cosine of the angle between adjacent unit vectors of velocity, averaged over a small region defined by R. This average is an operation over the measured velocity field $\mathbf{v}_{ij}(t)$:

$$\Phi_R(i,j,t) = \frac{1}{N_R} \sum_{(l,m)\in B_R(i,j)} \frac{\mathbf{v}_{ij}(t)\cdot\mathbf{v}_{lm}(t)}{|\mathbf{v}_{ij}(t)||\mathbf{v}_{lm}(t)|}, \qquad (5)$$

where $B_R(i,j)$ is a quasi circular region of radius R centered at (i,j) and N_R is the number of elements in such a set.

When $\Phi_R \sim 1$ the vectors inside the region B_R are nearly parallel. Values close to zero indicate strong misalignment. Negative values imply locally opposing streamlines. Resolution and noise level are determined by the choice of magnitude of R.

Standard correlation functions based on the velocity field, as in Fig. 4, hide long range continuities of correlation. Analyzing the streamline field in this novel way exhibits the global continuity of angular and polar correlations. The extent of the resultant sinuous domains depends on the choice of the averaging area $\sim R^2$. Large values of R produce a strong smoothing of the local data, which may hide the details of the chaotic nature of flow by means of statistical cancellations. Hence, small values of R should be preferred. But on the other hand, small values of R produce results that are more sensitive to noise in the raw data. They may be biased by the specific shape of the averaging region, connected to the fact that the grid chosen for the PIV is square. Fig. 5 shows the extent of continuous domains, derived from

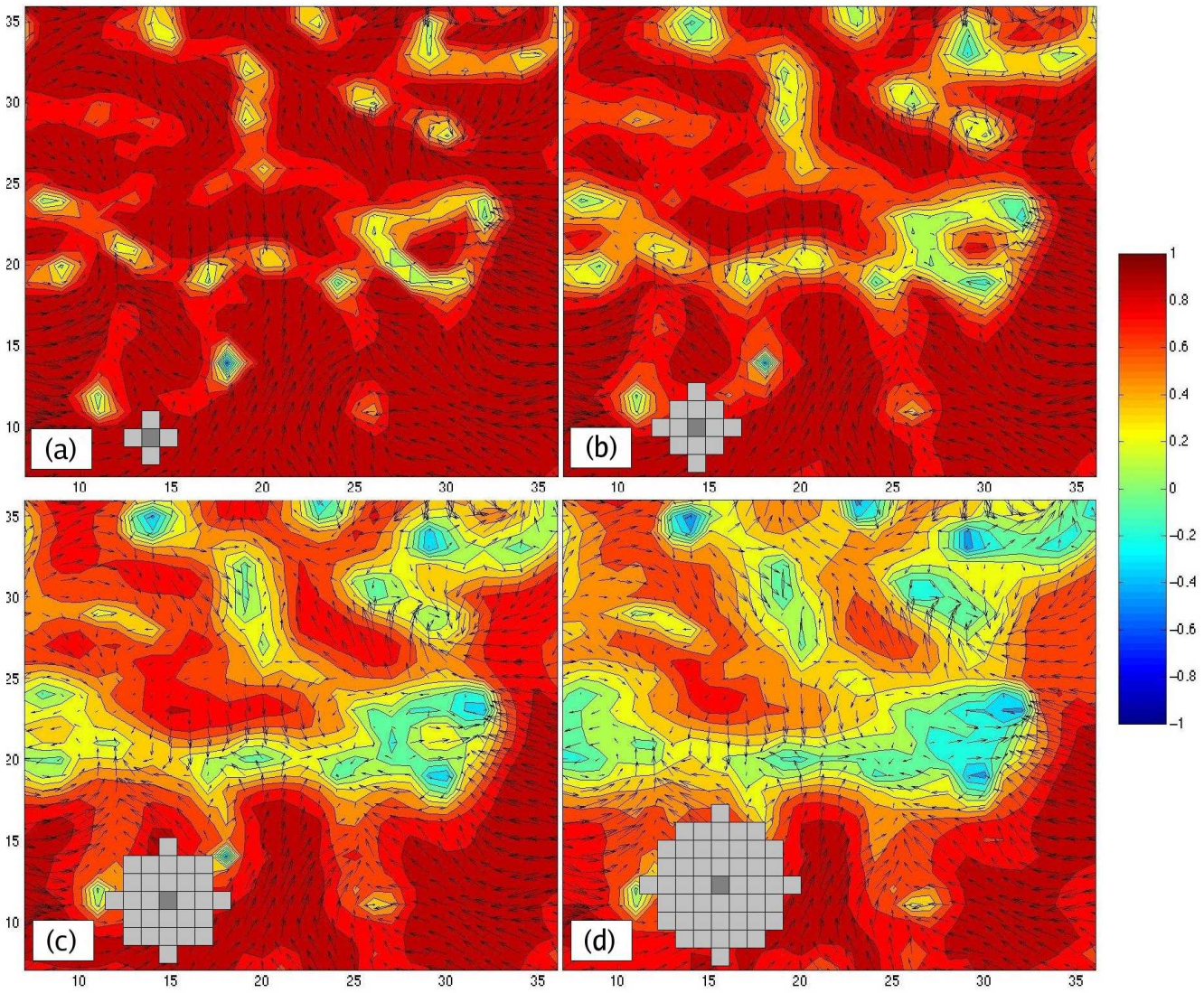

Fig. 5 Instantaneous coherence measure Φ_R (Eq. 5) for $R = 1$ (a), $R = 2$ (b), $R = 3$ (c) and $R = 4$ (d). Axes and R are in PIV grid units ($\simeq 2$ μm each). Gray boxes in the lower left corner indicate, in each case, the size and shape of the local averaging region used to estimate the measure. The color bar on the right indicate scale levels for values of Φ_R.

one data set, using different values of R. The red colored region corresponds to the level $0.8 < \Phi_R < 1$, which contours regions of high coherence. Inside these domains all speeds are parallel and co-directional within an angle slightly lower than 37 degrees.

For liquid crystals, the conventional order parameter involves $\langle(\cos\theta)^2\rangle$, thereby avoiding polarity. For the domains of coherent directional motion considered here, we can define the order parameter as

$$P_R(t) = \langle \Phi_R(t) \rangle, \tag{6}$$

where this average extends over the entire area, it i.e. all elements of the PIV image at time t. This quantity can be treated as a time series. We find that $P_R(t)$ has basically a stationary value with random fluctuations. Fig. 6 plots histograms of these order parameters. This method of analysis will be used in measuring the onset of the ZBN phase as a function of the concentration n.

What is the distribution of values of Φ_R in the whole field of view for each time step? What fraction of the total area in the levels map of Φ_R do they span? This approach asks for the probability of finding any given level of coherence in the flow, or the portion of the total that is spanned by each contour level on Fig. 5. These area fraction distributions are shown in Fig. 7 for four values of R. The data set in $[-1, 1]$ is partitioned in bins of size 0.2. We see an obvious shift of the center of the distribution when R is changed. Is interesting that each

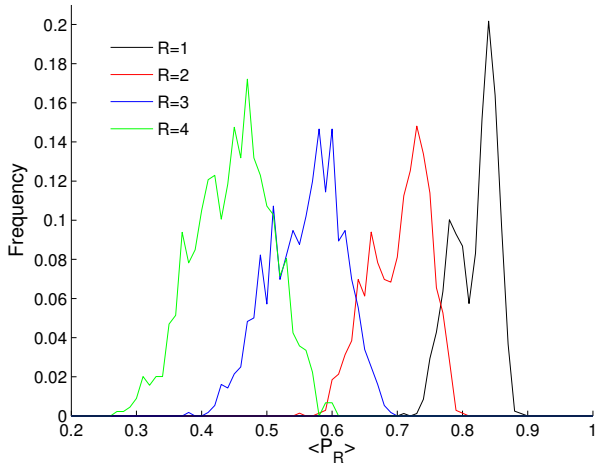

Fig. 6 Histograms for the order parameter $P_R(t)$ for different values of R. Each one is generated with 1000 time steps. The skewing of the distributions becoming two-peaked at low R (high resolution) presumably indicates the presence of a distribution of correlations.

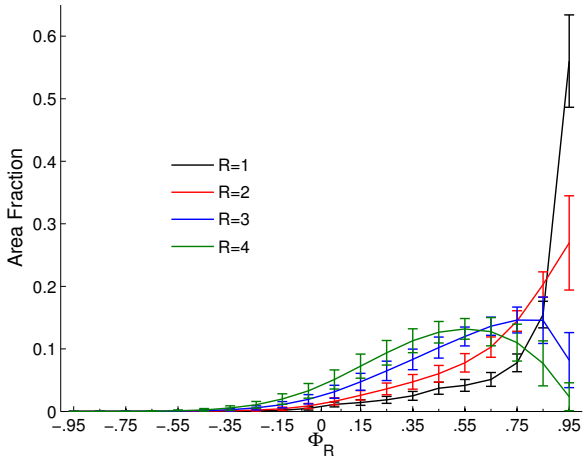

Fig. 7 Area fraction of coherent regions distributed over the whole range of Φ_R, averaged over 1000 time frames. Error bars indicate standard deviation in each case.

distribution is basically constant, meaning that the fraction of the system with a given coherent level stays more or less the same over time. This observation can yield a significant measure for understanding the process of organization of the system and give a hint of some type of stationarity in the system. It may tell that coherent regions are somehow stable. They deform, bend and may break apart, but the overall surface or volume stays more or less constant in time. Given that the suspension is approximately close-packed, it also implies that the number of cells in the aggregate of domains stays the same. The significance of this is that swimmers that are initially close-by tend to stay close along their path. The conservation of area fractions also suggests that the rate at which the coherent volume is moving into the focal plane is the same as the one leaving it. Then some "recycling" mechanism must be taking place in the perpendicular, out of focus, direction, like a bioconvection process. Another possibility could be that the whole dynamics is limited to a very narrow layer and is two dimensional. But this is not the case . We have observed that cells and clumps of cells or passive tracers tumble and move in and out of the focal plane, clearly proving that the dynamics is three-dimensional. Dynamics of recruiting and dropping of individuals into and out of phalanxes could be related to the topological details of this dynamic. There may be also implications for mixing and transport phenomena.

4 Recruiting into ZBN domains

Concentrated populations of *B. subtilis* spontaneously develop domains of the collective phase ZBN. Steric repulsion between cell bodies causes a nematic liquid crystal-like alignment that is demonstrated by the correlation of nearby angles, obtained from PIV analysis of the velocity field (Fig. 5). The axes of the cell bodies are aligned, but furthermore there is polarity, collective directional locomotion. Conventional nematics do not exhibit polar director axes. The recruiting of swimmers into a co-directionally swimming domain of cells, a phalanx, depends on three or more mechanisms. We have discovered, as discussed below, that individual cells of *B. subtilis* have a strong tendency to swim upstream in a shear flow. Such flows emerge from groups of co-directionally swimming cells. They provide a mechanism for recruiting more individuals into a phalanx. Another organizing/recruiting mechanism occurs when one of these bacteria encounters an obstacle. It can flip the propelling flagella from "back" to "front", resulting in reverse locomotion, without turning the bacterial cell body (Cisneros, *et al.*, 2006). This action may be a behavioral manifestation of flagellar dynamics and orientational instability. Paradoxically, it can aid polar alignment in groups, just because the individual cells are not themselves polar. Individual off-oriented cells can react by joining a colliding "obstacle", consisting of a moving phalanx of others. The transverse inward flows that surround a swimmer, or group of swimmers (Fig 13 and 14) provide yet another mechanism for recruiting, or coherence. These collectively generated currents can recruit adjacent organisms into pairs, multiplets, and eventually into domains of the ZBN. These flows, which are due to incompress-

ibility, are shown in section 5. A tightly knit group of propagating cells generates a backwash flow field, a lateral influx, and a flow forward, in the swimming direction.

Bacteria located near a rigid surface, in a prescribed shear flow, tend to swim upstream. Their trajectories, paths composed of swimming plus advection, are best observed at relatively low cell concentration. They consist of upstream segments, frequently of several seconds duration, sometimes of segments oriented across the flow, and intermittently of nearly passive downstream ones. Data were obtained on sixtyfive individual tracks that exhibit these characteristics, each modified by idiosyncratic details.

Swimming bacteria were suspended in Poiseuille flows within flat microslides (Vitrodynamics) with a 0.1 mm lumen. The velocity profile was determined by tracking 2 μm flourescent particles (Bangs Labs) near the focal plane. By comparing the out of focus beads to their images at known distances from the focal plane, the depth and velocity of the tracer particles can be used to determine the 3D velocity field and the shear. Cell trajectories in the up-swimming experiment were visualized by tracking the position of both ends of the cells through a sequence of images in the plane of focus. The vector orientation of a cell was determined from the distance between the ends of the cell and the angle. The angle and length give the projection of the cell body in the plane of focus. Velocity of the cells is calculated from the change in position of the cell from one frame to the next. This velocity represents the speed and direction that the cell is moving in the lab reference frame. Due to the external shear stress experienced by the cell the velocity vector does not necessarily pointing in the same direction as its orientation. The velocity of the fluid in the plane of focus can be subtracted giving the velocity of the cell in the reference frame of the fluid.

Figs. 8-10 show one representative trajectory, as observed, and relative to the fluid. This behavior of individual cells may be entirely hydrodynamic; a behavioral response to differential shear stress may also play a role. If up-swimming were due to chemotaxis, counter-current swimming would persist into the zero gradient region of the prescribed Poiseuille flow, which it does not. The interactions of cells and fluid velocity gradients, the deconvolution of cell path lines and fluid stream lines, and analysis of cell body orientation in relation to swimming direction are a current endeavor covering many such observations. Note that in Fig. 8 the cell body is oriented nearly transverse to the swimming direction. This orientation occurs in many cases, but not all. When it does, it implies the dissolution of the flagellar bundle, with individual flagella emerging approximately perpendicular to the body axis, as if driven by the fluid "wind" in which they operate. Our optical resolution is insufficient for ascertaining whether the cell bodies and flagella are at different levels in the shear field, a possible explanation of the phenomenon.

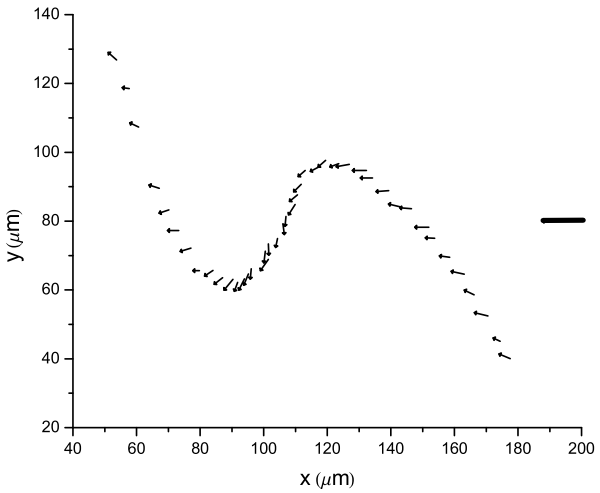

Fig. 8 Trajectory and *orientation* of a particular bacterial cell swimming in a flow, velocity in the positive y direction, with shear $dV_z/dz \sim 1.0$ sec^{-1}. The small arrows show the apparent swimming direction and the projection of the body size on the plane of observation. The bar on the right represents 20 micrometers.

5 Modeling self-propelled microorganisms

In the creeping flow regime where $Re \ll 1$, featuring linearity, superposition and time independence, a simple model of a self-propelled organism consists of two parts, a "body" **B** and an attached extendable "thruster" **T** that emerges from **B**. When forces within **B** provide an incremental backward push to **T**, the resulting increment of motion generates a surrounding field of fluid velocity. The motion of **B** is "forward" with velocity $\mathbf{V}_B$ relative to the surrounding stationary fluid; the motion of **T** is backward with velocity $\mathbf{V}_T$. The velocity with which **T** emerges from **B** is $\mathbf{v}_r$. Therefore, since **T** is attached to **B**,

$$\mathbf{V}_T = \mathbf{v}_r - \mathbf{V}_B.$$

When the respective drag coefficients are R_B and R_T, force balance is achieved when

$$F_B = R_B|\mathbf{V}_B| = R_T|\mathbf{v}_r - \mathbf{V}_B| = R_T|\mathbf{V}_T| = F_T, \quad (7)$$

where F_B and F_T are the forward and backward force magnitudes on the fluid.

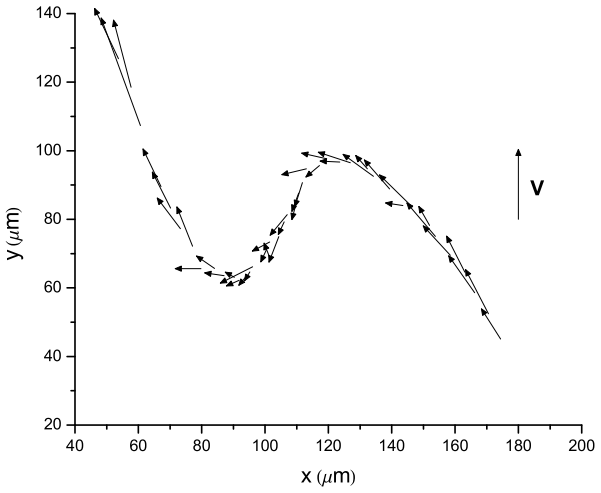

Fig. 9 Trajectory of the velocity vectors of the same bacterium as in Fig. 8 in the laboratory reference frame. The vector on the right side represents the fluid velocity of magnitude $\mathbf{V} = 78\mu$m/sec.

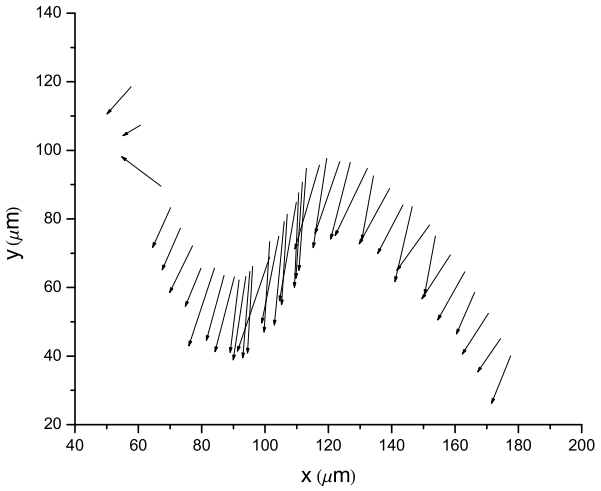

Fig. 10 The swimming velocity relative to the fluid, i.e. the local vectors shown in Fig. 9 minus the fluid velocity vector $\mathbf{V}$ with V = 78 μm/sec. Comparing with figures (8) and (9), note that the velocity of the bacterium can be transverse to its orientation.

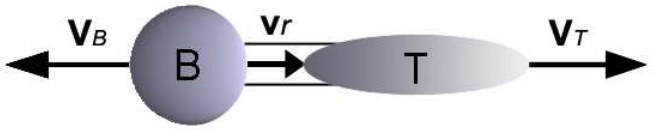

Fig. 11 Diagram of a model swimmer and velocities V_B and V_T induced on the fluid, and the velocity v_r of backward thrust of **T** out of **B**.

A schematic diagram of the swimmers and velocities is shown in Fig. 11, where the sphere and the ellipsoid indicate respectively **B** and **T**, which move with a relative velocity v_r.

For bacteria, **T** represents the rotating bundle of helical flagella. An increment of motion consists of a slight turn of the bundle during an increment of time. For the simplified case presented here, we ignore rotation. This model generates the salient features of the fluid flow field that surrounds a self-propelled organism or, by superposition, a group of organisms. It is not intended to elucidate the time development of trajectories. That objective would require a helical rotating thruster, or a magical putt-putt, where a thrust increment is followed by a drag-less increment of retraction.

The computational model presented below considers **B** a sphere and **T** a rod of finite diameter. Forward and backward velocities, calculated by force balance, are used to specify $\mathbf{V}_B$ and $\mathbf{V}_T$.

6 Flows and Forces

6.1 Sphere-stick model of a single organism

Each organism consists of one sphere (body **B**) of radius a_h and a cylinder (flagellum bundle **T**) of length ℓ and radius a_t along the z-axis, as depicted in Figure 12. The figure also shows an infinite plane wall which will be included in some of our computations. When the wall is present, it is located at $x_w = 0$. The head has velocity $(0, 0, V_B)$ and the tail has velocity $(0, 0, V_T)$. The balance of forces is achieved as follows. The drag force on an isolated sphere moving at velocity $(0, 0, V_B)$ is given by

$$\mathbf{F}_B = R_B \mathbf{V}_B = 6\pi\mu a_B V_B (0, 0, 1). \tag{8}$$

The force required to move the cylinder along its axis with velocity $(0, 0, V_T)$ is

$$\mathbf{F}_T = R_T \mathbf{V}_T = \frac{4\pi\mu\ell}{\ln(\ell^2/a_T^2) - 1} V_t (0, 0, 1). \tag{9}$$

For force balance we require $\mathbf{F}_B + \mathbf{F}_T = 0$ which results in

$$V_T = -\frac{3}{2}\frac{a_B}{\ell}\left[\ln(\ell^2/a_T^2) - 1\right] V_B. \tag{10}$$

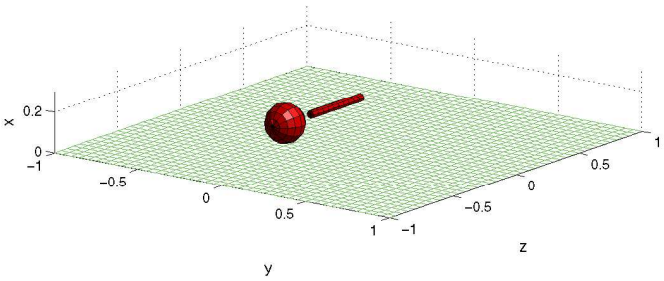

Fig. 12 Perspective view of the sphere-stick model and the wall.

6.2 Force computation

Given the instantaneous velocities of the head and tail of the organism, our goal is to compute the surface forces that produce these velocities at all the surface points. For this we use the method of Regularized Stokeslets (Cortez, 2001; Cortez, Fauci, & Medovikov, 2005). Briefly, the method assumes that each force is exerted not exclusively at a single point, but rather in a small sphere centered at a point $\mathbf{x}_k$. The force distribution is given by

$$\mathbf{F}(\mathbf{x}) = \mathbf{F}_k \phi(\mathbf{x} - \mathbf{x}_k), \tag{11}$$

where ϕ is a smooth narrow function (like a Gaussian) with total integral equal to 1. The limit of $\phi(\mathbf{x})$ as the width (given by a parameter ϵ) approaches zero is a Dirac delta $\delta(\mathbf{x})$. The role of the function ϕ is to de-singularize the velocity field that results from the application of a single force. For example, given a force $\mathbf{F}_k\phi(\mathbf{x})$ centered at $\mathbf{x}_k$ and using the regularizing function

$$\phi(\mathbf{x}) = \frac{15\epsilon^4}{8\pi(|\mathbf{x}|^2 + \epsilon^2)^{7/2}}, \tag{12}$$

the resulting velocity is

$$\mathbf{u}(\mathbf{x}) = \left(\frac{1}{8\pi\mu}\right) \frac{\mathbf{g}_k}{(|\mathbf{x} - \mathbf{x}_k|^2 + \epsilon^2)^{3/2}}, \tag{13}$$

where

$$\mathbf{g}_k = [|\mathbf{x} - \mathbf{x}_k|^2 + 2\epsilon^2]\mathbf{f}_k + [\mathbf{f}_k \cdot (\mathbf{x} - \mathbf{x}_k)](\mathbf{x} - \mathbf{x}_k)\ . \tag{14}$$

This is called a *Regularized Stokeslet* (Cortez, 2001 and Cortez *et al.*, 2005). Given a collection of forces distributed on a discrete set of points covering the surfaces of the sphere and cylinder, the resulting velocity obtained by superposition is

$$\mathbf{u}(\mathbf{x}) = \left(\frac{1}{8\pi\mu}\right) \sum_{k=1}^{N} \frac{\mathbf{g}_k}{(|\mathbf{x} - \mathbf{x}_k|^2 + \epsilon^2)^{3/2}}. \tag{15}$$

6.3 Boundary conditions:

For the computations with flow near an infinite plane wall, the boundary conditions of zero flow at the wall are enforced using the method of images. The image system required to exactly cancel the flow due to a singular Stokeslet was developed by Blake (Blake, 1971). It requires the use of a Stokeslet, a dipole and a doublet outside the fluid domain, below the wall. This system of images has been extended to the case of the regularized Stokeslet, Eq. 15.

6.4 Example 1: a single organism

We consider first a single organism moving parallel to an infinite plane wall. The table below shows the parameters used.

parameter	description
$a_h = 0.1$	radius of the head
$a_t = 0.02$	radius of the tail
$\ell = 0.4$	length of the tail
$U_h = -1.0$	velocity in the x-direction of the head
$U_t = 1.8718$	velocity in the x-direction of the tail

Since there is a linear relationship between the surface force and the fluid velocity, we set up a linear system of equations by evaluating Eq. 15 at all surface points and setting the velocities to their corresponding value. This leads to a linear system for the forces at all surface points. Once the forces are computed, the fluid flow at any point in the domain can be computed using again Eq. 15.

Figure 13 shows the fluid velocity on a plane parallel to the wall and through the organism as well as the flow on a plane through the organism and perpendicular to the wall. The contour lines are at 5%, 10%, 25%, 50%, 75% and 90% of the maximum fluid speed. Those contours give an idea of the extent of the fluid disturbance created by an organism. Figure 14 shows the streamlines of the instantaneous velocity field, revealing circulation patterns.

6.5 Example 2: two organisms

We next consider two organisms next to each other prescribed to move parallel to an infinite plane wall and to each other. The parameters are the same as those used in the previous example. Just as in the case of a single organism, the flow pattern suggests that the flow tends to "push" the organisms toward the wall and toward each other. This can be quantified by computing the forces exerted by the organisms on the fluid in order to move parallel to the wall and to each other.

Figure 15 shows the velocity field and the resulting forces exerted on the fluid by each of the two organisms. From the image, it is easy to see that there is a

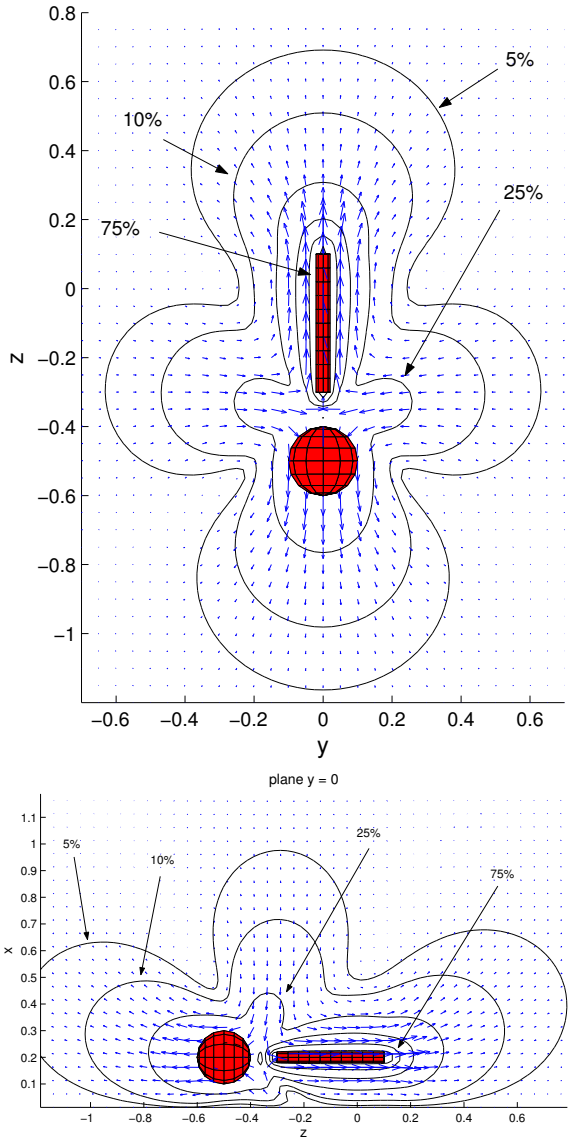

Fig. 13 Plan and side views of velocity field around one organism near a wall. The numbers indicate contours where the fluid speed is 5%, 10%, 25%, 50%, 75% and 90% of the maximum speed. The infinite plane wall is located at $x = 0$.

component of the force that points away from the wall, indicating that this components is needed to counteract the attraction effect of the wall in order to keep the organisms moving parallel to it. Similarly, the component of the force pointing away from the neighboring organism is required to counteract the attraction induced by the flow field.

6.6 Example 3: several organisms

We compute the flow around several organisms placed in a common plane above the wall. The velocity is computed also in that plane in order to visualize the effect of the prescribed motion of the group. Figure 16 shows the velocity field around the organisms and a close-up view of the flow between some of the organisms, while Fig. 17) shows the streamlines for the same configuration.

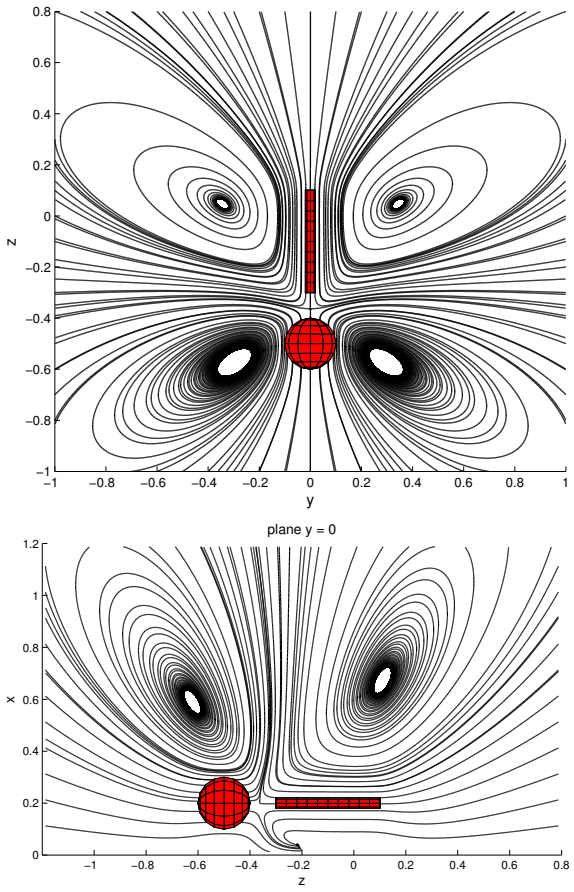

Fig. 14 Streamlines of the velocity field around one organism near a wall. Plan and side views.

6.7 Significance of Computational Results

The computed geometries and magnitudes of the flows generated by the locomotion provide some understanding of the forces between swimming organisms and between organisms and adjacent no-slip surfaces. We observe, in experiments, that two or more bacteria swimming near each other, co-directionally, continue for long distances in these parallel paths. The computed forces on each swimmer, shown in Fig. 15, show the attraction of the cells to each other and to the nearby plane. Additional computations show that in the absence of the plane, the vertical components vanish (by symmetry), and the horizontal attractive components diminish. The attractive force is due to transverse flow toward the organism axis (Fig. 13), required by conservation of volume: the body propels water forward, the tail pushes

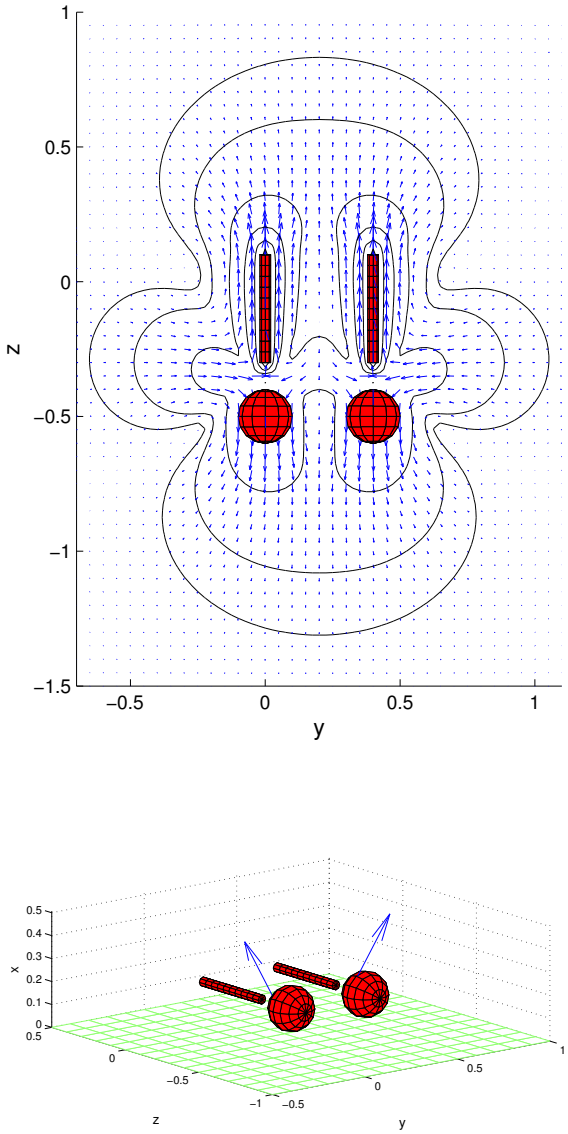

Fig. 15 Velocity field around two organisms near a wall and resultant forces exerted by each organism on the fluid in order to move parallel to the wall and to each other. The forces are $(2.72, -1.71, -0.22)|\mathbf{F}_B|$ (left organism) and $(2.72, 1.71, -0.22)|\mathbf{F}_B|$ (right organism), where $\mathbf{F}_B$ is the drag on the sphere given by Eq. 8.

water backward, leaving a central region of inflow due to lowered pressure. In the absence of the nearby plane, the influx is weaker because of spherical symmetry. The same influx can be seen toward the centers (between body and tail) of organisms which are members of a multi-organism phalanx (Fig. 16). Transverse flows between the body of a follower and the tail of a preceder are also seen in the upper image of Fig. 16. Whether a sum over transverse flows in a 3D domain consisting of many close-packed organisms provides net lateral/radial cohesion remains to be seen.

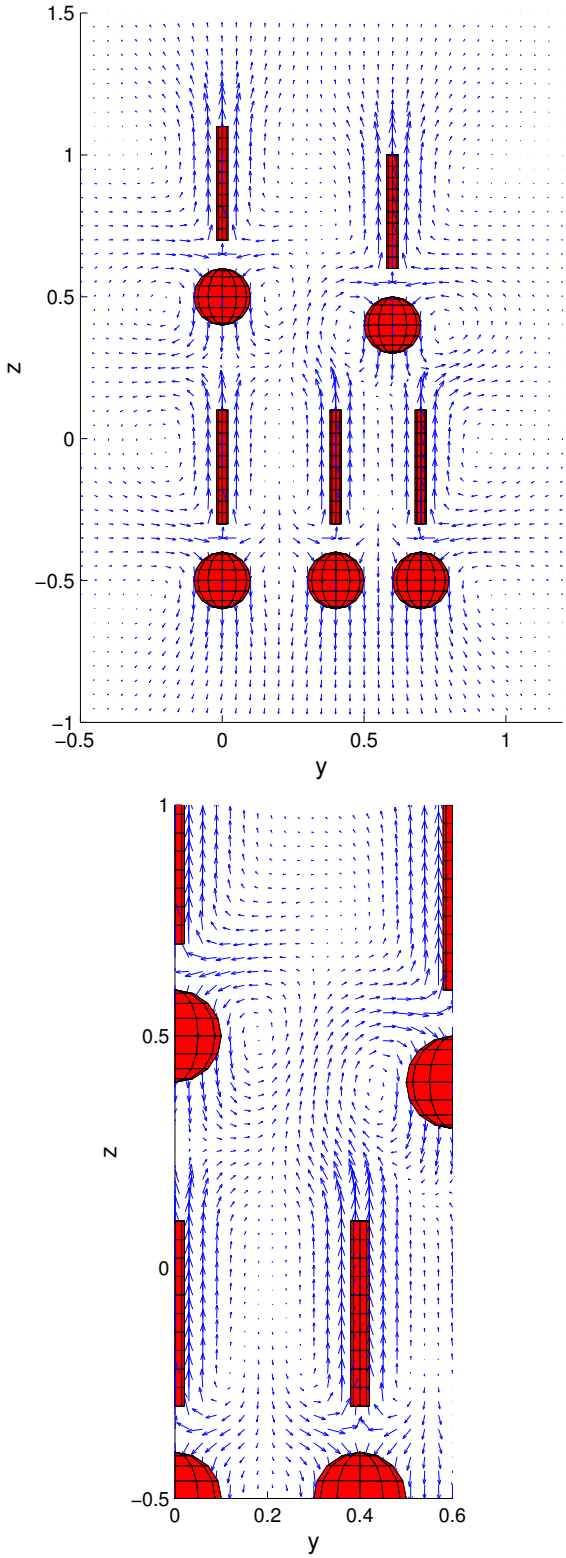

Fig. 16 Velocity field around several organisms above a wall (top) and a closer view of the velocity between them (bottom).

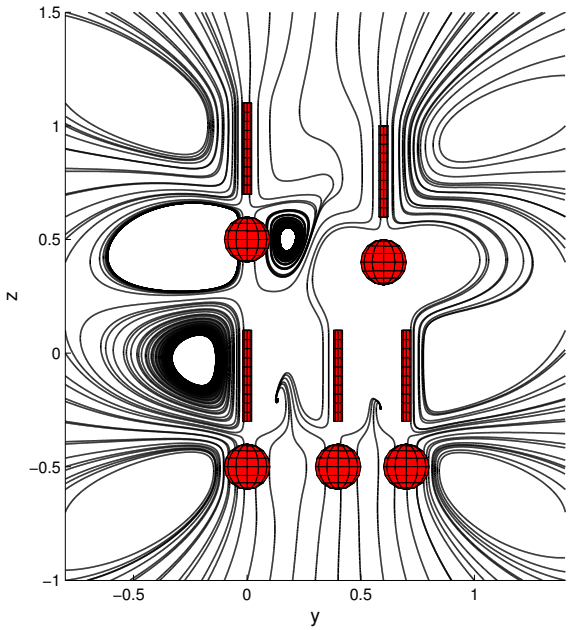

Fig. 17 Streamlines of the velocity field around several organisms near and above a wall. The flow is the same as that in Fig. 16.

Figs 16 and 17 also show the flows that penetrate or surround a group. It is evident that there is very little front-to-back penetration of fluid. The exchange is mostly lateral. The leading heads push water forward, the tail-end cells push water backward, generating much of the collective forward propulsion. The low velocities of flow in the interior (the lower images of Fig. 16 and Fig. 17) imply compensating forces and relatively little advective communication between cells, as discussed in the introduction. Similar calculations have been performed on groups of ten cells, and on staggered pairs. The associated interior flows are weak, but vortical regions, as in Fig 17, or even more spectacular, can provide significantly enhanced transport of suspended particles or molecules.

More extensive results have been obtained. They will be reported in a separate paper, currently in preparation. The results presented here show some of the fundamental ingredients required for understanding the hydrodynamics of collective behavior.

7 Turbulence at $Re \ll 1$?

To the casual observer, the ZBN phase of a concentrated suspension of swimming *B. subtilis* appears turbulent. More quantitatively, the analysis of the collective dynamics, using PIV based on the motion of the bacteria, or on passive tracers, exhibits some features of turbulence. Furthermore, the collective velocities of coherent subpopulations of bacteria can be greater than the swimming velocities of individual cells. Considering the suspension as a simple fluid, the conventional Reynolds number,

$$Re = \frac{UL}{\nu},$$

where ν is the kinematic viscosity, U is a mean collective velocity, $U \sim 5 \times 10^{-3}$ cm/sec, $L \sim 10^{-2}$ cm is a typical correlation length (Fig 4). Thus, $Re \ll 1$ for typical values of $\nu \sim 10^{-2}$ cm^2/sec. An increase of ν due to suspension effects further decreases Re. The how can the quasi-turbulence be sustained?

One can analyze the observed dynamics by considering the force or power densities produced by the swimming organisms. The conventional Reynolds number is the ratio between kinetic energy and viscous dissipation. An analogous dimensionless ratio can be constructed from the Stokes force that a single bacterial cell must exert to move itself at velocity $\mathbf{v}$,

$$\mathbf{f} = c\mu a\mathbf{v}, \tag{16}$$

where a is the radius, μ is the viscosity of the medium and c is a geometrical factor of order 10^1. In particular, for a sphere in an infinite medium $c = 6\pi$ (Stokes sphere).

The power put by a cell into the suspension that surrounds it is $P_n = \mathbf{f} \cdot \mathbf{v} = c\mu a v^2$; for a concentration of n cells per unit volume

$$P_n = cn\mu a v^2 \tag{17}$$

is the total power input density. The viscous dissipation of power in the collective phase is estimated as

$$P_\mu = \mu \left(\frac{\mathbf{U}}{L} \right)^2, \tag{18}$$

where $\mu U/L$ is the collective shear stress and U/L is a characteristic time. Then, based on these energy arguments, the dimensionless ratio "Bacterial swimming number", B_{se} is defined as

$$B_{se} = \frac{P_n}{P_\mu} = cnL^2 a \left(\frac{v}{U} \right)^2. \tag{19}$$

For the nearly close-packed ZBN phase, $n \sim 10^{11}$cm^{-3}. Taking the velocity ratio of order unity, a of order 10^{-4} cm, and $L \approx 10^{-2}$ cm, the observed correlation length, $B_{se} \sim 10^4$. This "alternative" Reynolds number explains the possibility of a turbulent dynamics when $Re \ll 1$. The large magnitude of B_{se} sweeps away details on the assumptions of parameters values.

This result can also be obtained via the standard non-dimensionalization of the Navier-Stokes equation with an included force/volume exerted by the swimming organisms. Hence, the fluid flow $\mathbf{u}$ is described by

$$\rho \frac{D\mathbf{u}}{Dt} = \mu \nabla^2 \mathbf{u} - \nabla p + cn\mu a \mathbf{v} \gamma \tag{20}$$

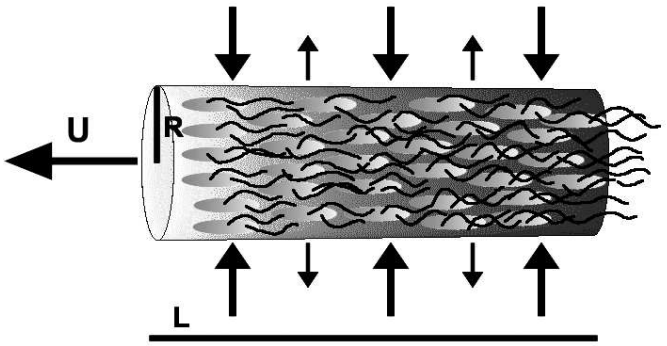

Fig. 18 Schematic diagram of a phalanx, a coherent domain of cells swimming to the left with collective velocity **U**. Arrows indicate direction of transverse fluid flow as in Figs. 16 and 17 due to the collective motion inside the domain.

where ρ is the mean density of the suspension and γ is a function that models the propulsive force of one organism. Dividing this equation by the term $\mu U/L^2$ delivers a new dimensionless number B_s, based on stresses, as the magnitude of the forcing term:

$$B_s = c(n\mu a)\frac{|\mathbf{v}|}{(\mu U/L^2)}\gamma = c(nL^2a)\left(\frac{v}{U}\right)\gamma \qquad (21)$$

This can also be written as:

$$B_s = cq\left(\frac{v}{U}\right)\gamma \qquad (22)$$

with $q \equiv (nL^2a)$ a dimensionless factor.

This dimensionless ratio is essentially the same as the B_{se} number, except that now U and L ought to arise out of equation (20) as parameters that give a particular scale to the system. Note that both B_s and B_{se} are essentially geometric factors, the viscosity having cancelled (Tuval, *et al*, 2005).

The function γ accounts for the fact that a single organism exerts on the fluid equal and opposite forces, displaced by approximately one organism length. Eq. 20 presumably applies only to the case of rather low concentrations of bacteria. The dimensional analysis yielding B_{se} is not concentration dependent.

We now sketch a the outlines of a model that uses the results of experiments together with an extrapolation of the calculation results in the previous section, e.g. Figs. 16 and 17. To estimate the collective velocity U of a domain, we consider a cylinder of aligned co-directionally swimming bacteria each swimming with the mean velocity **v** (Fig. 18). The propulsion of the cylindrical domain is due to the forces exerted on the fluid by the flagella emerging from one or more layers of cells at the rear of the cylinder. The bodies of cells at the front push fluid forward. Transverse flows enter and leave the side of the cylinder, with presumably a net volume conserving, also temporarily stabilizing influx. The concentration of bacteria per area is $n^{2/3}$, the area is πR^2, and S layers of cells contribute the force F_0 (Eq. 16). Assuming the drag of the cylinder is $C\mu LU$, we conclude

$$U = \left(\frac{\pi c}{C}\right)\left(\frac{SR^2an^{2/3}}{L}\right)v. \qquad (23)$$

For $R = 10^{-3}$cm, $L = 10^{-2}$cm, $a = 10^{-6}$cm, $n^{2/3} = 2 \cdot 10^7\text{cm}^{-2}$ and $S\pi c/C = 10$, $U = 1.8v$, indicating that a more formal version of this approach may prove useful.

8 Discussion

8.1 Background

Convective dynamics driven by microorganisms, especially swimming cells of monocellular algae, have been summarized by Pedley and Kessler (1992) and Hill and Pedley (2005). Much of that data and the mathematical modelling associated with it relates to gravity driven bioconvection of suspensions of monocellular algae, plants that swim upward: toward light, and/or because of orientation of the cells in the earth's gravitational field. The initial volume fraction was fairly low in these situations, e.g $\approx 10^{-3}$ or less. Theoretical approaches could therefore use Navier-Stokes equations that included a smoothed gravitational body force proportional to the concentration of organisms and their mass density. An additional equation modelled transport of organisms due to swimming and advection by the flow. Ramia et al. (1993) published an excellent theory of locomotion for micro-organisms with a single flagellum. Nasseri and Phan-Thien (1997) showed that abjacent swimmers interact hydrodynamically.

The respiration of the bacteria *B. subtilis* depletes dissolved oxygen. Transport from an interface between the aqueous suspension of these cells and the surrounding air replenishes it. Bacteria swim up the resultant gradient of oxygen concentration. In a shallow suspension the cells swim upward, toward the air. Accumulation at the interface results in an unstable gradient of mean fluid density, since the bacteria are approximately 10% denser than water. This system was modelled by partial differential equations that coupled hydrodynamics, consumption, and transport of oxygen and cells (Hillesdon *et al.*, 1995; Hillesdon and Pedley, 1996; Tuval *et al.* 2005). When geometric constraints inhibit bioconvection or other means of dispersal, it was discovered that the concentrated accumulation of cells supports the remarkable collective dynamics that are the subject of this paper (Kessler and Wojciechowski, 1997) and (Kessler and Hill, 1997). Mendelson et al. (1999) reported closely related phenomena, jets and whirls, that occur near the edges of bacterial cultures that grow and expand on wet agar surfaces. Wu and Libchaber (2000) and Sokolov, *et al.* (2006) demonstrated a new version of the phenomenon when concentrated bacterial populations are trapped in suspended thin aqueous films.

Lega and Mendelson (1999), Simha and Ramaswamy (2002), Lega and Passot (2003) and Hernandez-Ortiz, *et al.* (2005) have described analyses of data and approaches toward a theory.

8.2 Results and Questions

This paper shows how hydrodynamics and behavior of a concentrated population of swimming microorganisms can combine to form a collective dynamic, the Zooming BioNematic (ZBN), consisting of interacting nematic liquid crystal-like domains that exhibit quorum polarity of propagation with spatial and temporal correlation. Relevant experiments on individual cell motility, and a novel approach for understanding locomotion and for calculating the flows that surround swimmers provide ingredients for a realistic theoretical model of this complex two phase system. Dimensional analysis demonstrates that the observed speeds of the collective domains are plausible, and that the occurrence of turbulence-like dynamics at $Re \ll 1$ can be understood by considering the input of (swimming) energy from the occupants of the fluid.

We demonstrate that the results of PIV, obtained from high speed cine microscope images of the swimming cells, i.e. under difficult circumstances, can provide useful data on velocity and vorticity distributions, the latter exhibiting a rather satisfying alternation of signs, somewhat like vortex streets. It should be remembered that the PIV data were obtained from the bacteria, the solid suspended phase, not from the water. We developed a novel measure of angular alignment (and deviation), based on the velocity vector field. That analysis showed the remarkable spatial extent of continuous alignment, as well as singular regions of defect. Whereas averages over many quasi-instantaneous correlations of vorticity and velocity showed decays of order one second, the alignment data exhibited remarkable stability.

Transport of biologically significant molecules, for cell-cell communication, for supply of nutrients and elimination of wastes, and for respiration can be greatly enhanced by the chaotic advection that accompanies the intermittent collisions, reconstitution and decay of the zooming domains. Proceeding from there: We believe that we generate reasonable insights concerning the formation of propagating coherent regions. Ingredients for formation are the transverse flows and inward forces that accompany swimming Fig. 15, up-flow swimming in shear flows (section 4), flipping of flagella at obstacles (Cisneros, *et al.*, 2006), and of course geometrically determined stacking (steric repulsion).

What determines the breakup of domains? Extrapolating from Fig. 16 and calculations, not shown here, for phalanxes comprising more swimmers, the flow inside a domain is quite weak. The supply of oxygen to the interior cells (note Fig. 17) will be insufficient to maintain average levels of concentration. The interior cells will therefore swim transversely, up the gradient of oxygen concentration, or swim ever more slowly; both scenarios imply breakup. The swimming velocity distribution of individual cells is approximately Maxwellian, and very oxygen dependent (Kessler and Wojciechowski, 1997). The uniform speed of cells in phalanxes is therefore quite remarkable. The decay time of averaged correlations is about one second (Fig. 4) and oxygen supply times (last paragraph, section 1) are about the same. Coincidence? Probably not. There are other possible contributors to decay of coherence. Interior cells may begin tumbling, in search of a more favorable chemical environment; phalanxes that collide break up; the head end of elongated domains, as in Fig. 18, may buckle (we occasionally observe very explicit cases of roll-up); instability of nematics (Simha and Ramaswamy, 2002) may also be a factor. The intermittency problem clearly needs further work.

9 Acknowledgements

This research has been supported by DOE W31-109-ENG38 and NSF PHY 0551742. We should like especially to thank Matti M. Laetsch for her contributions to Section 4, and to David Bentley for help with Fig. 1.

References

1. Berg H.C. (2003) E. coli in Motion. 1st ed., New York: Springer.
2. Berg H.C. (1993) Random Walks in Biology. Rv/Nw/Expn ed., Princeton: Princeton University Press
3. Blake J.R. (1971) A Note on the the image system for a stokeslet in a no-slip boundary. Proc. Camb. Phil. Soc. 70:303
4. Cisneros L., Dombrowski C., Goldstein R.E. and Kessler J.O. (2006) Reversal of bacterial locomotion at an obstacle. Phys. Rev. E,73: 030901-4
5. Childress S. (1981) Mechanics of swimming and flying, Cambridge, UK: Cambridge University Press,
6. Cortez R. (2001) The method of regularized Sokeslets. SIAM J. Sci. Comput. 23(4):1204-1225
7. Cortez R., Fauci L. and Medovikov A. (2005) The method of regularized Stokeslets in Three Dimensions: Analysis, Validation and Application to Helical Swimming. Phys. Fl., 17:1–14
8. de Gennes P.G. and Prost J. (1993) The Physics of Liquid Crystals, Oxford: Oxford University Press
9. Dombrowski C., Cisneros L., Chatkaew S., Goldstein R.E. and Kessler J.O. (2004) Self-Concentration and Large-Scale Coherence in Bacterial Dynamics. Phys. Rev. Lett. 93: 098103-4
10. Hill N.A. and Pedley T.J. (2005) Bioconvection. Fl. Dyn. R. 37: 1-20
11. Hillesdon AJ, Pedley TJ (1996) Bioconvection in suspensions of oxytactic bacteria: Linear theory. Journal of Fluid Mechanics 324: 223-259.
12. Hillesdon A.J., Pedley T.J., Kessler J.O. (1995) The development of concentration gradients in a suspension of chemotactic bacteria. Bulletin of Mathematical Biology. 57 (2): 299

13. Hernandez-Ortiz J.P., Stoltz C.G. and Graham M.D. (2005) Transport and Collective Dynamics in Suspensions of Confined Swimming Particles. Phys. Rev. Lett. 95: 204501
14. Keane R.D. and Adrian R. (1992) Theory of cross- correlation analysis of PIV images. App. Sc. R. 49: 191
15. Kessler J.O. and Hill N.A. (1997) Complementarity of Physics, Biology and Geometry in the dynamics of swimming micro-organisms. In: In Physics of Biological Systems. Springer Lecture Notes in Physics 480:325 - 340 (ed H. Flyvbjerg, et al), Berlin: Springer Verlag
16. Kessler J.O. and Wojciechowski M.F. (1997) Collective Behavior and Dynamics of Swimming Bacteria. In: Bacteria as Multicellular Organisms. pp 417 - 450 (ed Shapiro J.A. and Dworkin M.), New York: Oxford University Press
17. Kolter R. and Greenberg E.P. (2006) Microbial Sciences. The superficial life of microbes. Nature 441: 300-302
18. Lega J., Mendelson N.H. (1999) Control-parameter-dependent Swift-Hohenberg equation as a model for bioconvection patterns. Phys. Rev. E. 59 (6): 6267-6274
19. Lega J., Passot T. (2003) Hydrodynamics of bacterial colonies: A model. Phys. Rev. E. 67(3):031906
20. Lighthill M.J. (1975) Mathematical biofluiddynamics, SIAM, Philadelphia
21. Magariyama Y., Sugiyama S., Muramoto K., Kawagishi I., Imae Y. and Kudo S. (1995) Simultaneous measurement of bacterial flagellar rotation rate and swimming speed. Biophys. J. 69: 2154-2162
22. Magariyama Y., Sugiyama S., Kudo S. (2001) Bacterial swimming speed and rotation rate of bundled flagella. FEMS Microbiol. Lett. 199:125-129
23. Mendelson N.H., Bourque A., Wilkening K., Anderson K.R. and Watkins J.C., (1999) Organized cell swimming motions in in Bacillus subtilis colonies: Patterns of short-lived whirls and jets. J. Bact. 181: 600-609
24. Miller M.B. and Bassler B.L. (2001) Quorum Sensing in Bacteria. Ann. Rev. of Microbiol.. 55:165-199
25. Nasseri S, PhanThien N (1997). Hydrodynamic interaction between two nearby swimming micromachines. Computational Mechanics. 20 (6): 551-559
26. Pedley T.J. and Kessler J.O. (1992) Hydrodynamic Phenomena in Suspensions of Swimming Microorganisms. Ann. Rev. Fl. Mech. 24: 313-358
27. Pozrikidis C. (1997) Introduction to Theoretical and Computational Fluid Dynamics. New York : Oxford University Press
28. Ramia M., Tullock D.L., Phan-Thien N. (1993) The role of hydrodynamic interaction in the locomotion of microorganisms. Biophys. J. 65 (2): 755-778
29. Simha R.A., Ramaswamy S. (2002) Hydrodynamic fluctuations and instabilities in ordered suspensions of self-propelled particles. Phys. Rev. Lett. 89:058101
30. Simha R.A., Ramaswamy S. (2002) Statistical hydrodynamics of ordered suspensions of self-propelled particles: waves, giant number fluctuations and instabilities. Physica A. 306(1-4): 262-269
31. Short M.B., Solari C.A., Ganguly S., Powers T.R., Kessler J.O., Goldstein R.E. (2006) Flows Driven by Flagella of Multicellular Organisms Enhance Long-Range Molecular Transport. P.N.A.S (USA) 103, 8315-8319
32. Solari C., Kessler JO, Goldstein RE (2006) Motility, Mixing, and Multicellularity. Developmental Systems of Genetic Programming and Evolvable Machines (Preprint)
33. Tuval I., Cisneros L., Dombrowski C., Wolgemuth C.W., Kessler J.O. and Goldstein R.E. (2005) Bacterial swimming and oxygen transport near contact lines. P.N.A.S., 102: 2277-2282
34. Willert C.E. and Gharib M. (1991) Digital particle image velocimetry. Exp. Fl. 10: 181
35. Wu, T. (Y.-T.) et al. (1975) Swimming and flying in nature, New York: Plenum Press
36. Wu X.L., Libchaber A. (2000) Particle diffusion in a quasi-two-dimensional bacterial bath. Phys. Rev. Lett. 84(13): 3017-3020